JOURNAL OF CATALYSIS 84, 200–215 (1983)

Reduction of NO by CO over Silica-Supported Rhodium: Infrared and Kinetic Studies

WILLIAM C. HECKER[1] AND ALEXIS T. BELL

Department of Chemical Engineering, University of California, Berkeley, California 94720

Received April 12, 1983; revised June 13, 1983

The kinetics of NO reduction by CO have been investigated over a Rh/SiO_2 catalyst. These studies have been complemented by *in situ* infrared studies. The specific activity is found to be sensitive to the nature of the catalyst pretreatment. Preoxidation in NO increases the specific activity for NO reduction by 50% over that observed when the catalyst is prereduced. Pretreatment has little effect, though, on the selectivity for forming N_2 versus N_2O. For NO conversions below 50%, the kinetics for NO reduction, and for N_2 and N_2O formation, are positive order in CO but inverse order in NO. The activation energies for all three processes are equivalent. Infrared spectra taken under reaction conditions show that the surface is nearly saturated by adsorbed NO. Smaller coverages by CO and NCO species are also observed. The results of both the spectroscopic and rate studies can be interpreted on the basis of a relatively simple reaction mechanism. The rate-limiting step in this model is assumed to be the dissociation of chemisorbed NO. The higher specific activity for NO reduction observed upon preoxidation of the catalyst is ascribed to the more facile dissociation of adsorbed NO on a partially oxidized Rh surface.

INTRODUCTION

Rhodium is currently added to automotive exhaust catalysts in order to control the emissions of NO_x (*1*). The selection of Rh was based on screening studies (*1–3*) which demonstrated that Rh is more effective than Pt and Pd for promoting the reduction of NO under conditions of near stoichiometric combustion. While Ru is even more active than Rh, and produces less NH_3, it is unstable since it forms a volatile oxide. In view of the fact that exhaust gas conversion constitutes one of the world's largest catalytic processes, there has been considerable interest in understanding the mechanism and kinetics of individual processes occurring on the catalyst surface (*1, 4–6*). The objectives of this investigation were to establish the kinetics of NO reduction by CO over Rh and to combine this information with *in situ* infrared observations for the purpose of gaining further insight into the reduction mechanism.

The interactions of NO and CO with Rh have been investigated previously through the use of infrared spectroscopy and temperature-programmed desorption (TPD) spectroscopy. Infrared studies (*7–9*) show that there are three major forms of adsorbed NO: a cationic species, $Rh–NO^{\delta+}$, characterized by a band at 1910 cm^{-1}; a neutral species Rh–NO, characterized by a band at 1830 cm^{-1}; and an anionic species, $Rh–NO^{\delta-}$, characterized by a band at 1690 to 1630 cm^{-1}. Three forms of adsorbed CO have also been identified (*10–13*): a linear species Rh–CO, characterized by a band near 2060 cm^{-1}; a bridged species, Rh_2CO, characterized by a band lying between 1930 and 1860 cm^{-1}; and a *gem*-dicarbonyl species, $Rh(CO)_2$, characterized by bands at 2100 and 2035 cm^{-1}. When NO and CO are coadsorbed, the features characteristic of NO tend to dominate over those for CO indicating that NO is more strongly adsorbed than CO.

[1] Current address: Department of Chemical Engineering, Brigham Young University, Provo, Utah 84602.

0021-9517/83 $3.00

TPD studies of both supported (*14*) and unsupported (*15–17*) Rh show that NO readily decomposes at elevated temperatures to produce N_2 and N_2O. The oxygen released by decomposition is very strongly bound and does not desorb until the catalyst temperature exceeds the temperature at which nitrogen-containing products are formed. The decomposition of NO is considered to begin with the dissociation of adsorbed NO (*14–17*). N_2O is formed by the reaction of adsorbed NO and N atoms. The formation of N_2 is thought to occur via two processes (*14*), a low temperature process represented by $NO_a + N_a \rightarrow N_2 + O_a + S$ and a high temperature process represented by $2N_a \rightarrow N_2 + 2S$.

EXPERIMENTAL METHODS

Apparatus. The apparatus used for the work reported here is similar to that used previously (*18–20*) and is described in detail in Ref. (*21*). The central component is a heated infrared reactor made of 304 stainless steel. The reactor is comprised of two chambers connected in series. One of these chambers contains a disk of catalyst, and the other chamber an equivalent disk of the support. The circular openings cut into each chamber to permit passage of an infrared beam are covered by CaF_2 windows. The reactor sits in the sample compartment of a Perkin–Elmer 467 infrared spectrometer. The orientation of the two chambers is such that the sample beam passes through the catalyst disk and the reference beam through the support disk. By this means, infrared bands characteristic of the support and gas phase can be subtracted from the spectrum of the catalyst sample, to emphasize spectral features due to adsorbed species.

To minimize the blank activity due to the catalytic properties of stainless steel, the internal surfaces of the reactor were coated with aluminum where possible. Upon exposure to air, this coating developed a thin layer of aluminum oxide. The activity of the empty reactor was tested prior to putting it into service. Using a feed containing 3% CO and 1% NO in helium, flowing at 200 STP cm^3/min, no detectable conversion of NO was observed at temperatures between 473 and 536 K. Raising the temperature to 558 K resulted in a conversion of 0.4%. This is considerably less than the 100% conversion observed when the reactor contained 0.123 g of the catalyst.

The reactor was connected to a gas recycle loop containing a preheater upstream of the reactor and a forced air-cooled coil downstream of the reactor. To minimize background activity, both the preheater and cooling coil were made of aluminum tubing (alloy T6061). Gas flow in the loop was provided by a 40-liters/min stainless-steel bellows pump. Reactants were continually fed into, and products were withdrawn from, the recirculating gases. With a nominal flow rate of 200 cm^3/min to the loop, a recycle ratio of 200 : 1 could be achieved, allowing the reactor to be characterized as a CSTR.

The reaction products were analyzed using the gas chromatographic system described by Hecker and Bell (*22*). This system uses two columns to separate NO, N_2, N_2O, CO, and CO_2. Data acquisition and reduction were carried out by means of a microprocessor. The program used for data reduction also checks the nitrogen balance. With this system, gas analyses could be obtained once every 10 min and nitrogen balances were found to lie routinely within $\pm 0.1\%$ of expected stoichiometry.

Materials. A 4.6% Rh/SiO_2 catalyst was prepared by incipient wetness impregnation of Cab-O-Sil HS-5 with an aqueous solution of $RhCl_3 \cdot 3H_2O$. The resulting mixture was dried in a vacuum oven and then calcined in air for 1 h at 773 K. The catalyst was then reduced in flowing H_2 at 673 K for ~2 h and at 573 K for an additional 16 h. The dispersion of the reduced catalyst was determined to be 38%, by means of H_2 chemisorption. A 29-mm-diameter disk of the catalyst, weighing 0.123 g, was prepared by pressing a 120-mesh cut of the catalyst in a special die made of tool steel.

All gases were purified prior to use. Helium (99.998%) was passed through an Oxyclear unit (Labclear) followed by a bed of molecular sieve. Hydrogen (99.999%) was purified by passage through a Deoxo unit (Engelhard) followed by a bed of molecular sieve. These procedures served to remove oxygen and water from each gas. Carbon monoxide (99.9%) was freed of iron carbonyl and carbon dioxide by passage through a heated tube packed with glass beads, followed by an ascarite trap. The nitric oxide used for these studies was in the form of either 6.15 or 11.5% NO mixtures in helium. These mixtures were found to contain several hundred parts per million of N_2O and N_2 as impurities. The N_2O was removed by passage of the gas through a molecular sieve trap. The N_2 impurity could not be removed, but was accounted for in determining the rate of N_2 produced during NO reduction.

RESULTS

Rate Measurements

Preceding each run, the catalyst was either reduced in H_2 or oxidized in NO. Reduction was typically done at 553–573 K in 100% H_2 for at least 24 h. Oxidation was carried out for 1 to 2 h at the temperature of the subsequent run, using a 1–2% NO mixture in helium. The pretreatment period was ended by purging the reactor loop with helium, usually for 15–60 min.

Following pretreatment and prior to collecting rate data, the reaction of NO and CO was allowed to proceed for a period of 15–20 h. It was observed that the catalyst activity underwent a moderate decay in the first 3–5 h of this period, and then slowly approached steady-state performance. The 15- to 20-h break-in period assured that rate data were taken under steady-state conditions.

The nature of the catalyst pretreatment has a significant effect on the steady-state activity of the catalyst. As shown in Fig. 1, preoxidation of the catalyst results in a 50% higher NO reduction activity than when the catalyst is prereduced. The magnitude of this effect is independent of both NO and CO partial pressures, and is also independent of temperature over the range of 463 to 523 K. Figure 2 shows that catalyst pre-

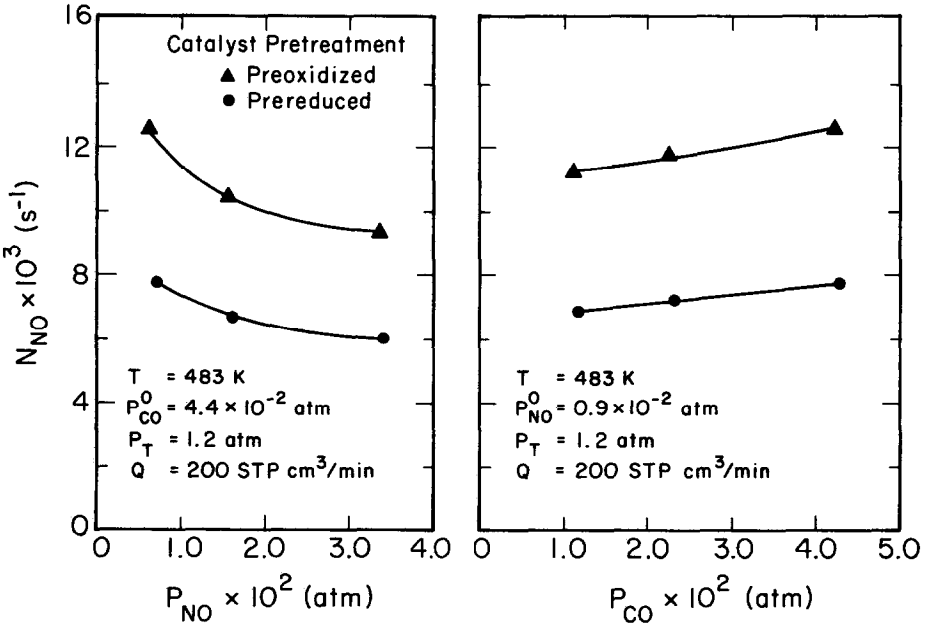

FIG. 1. Effect of pretreatment on the turnover frequency for NO reduction.

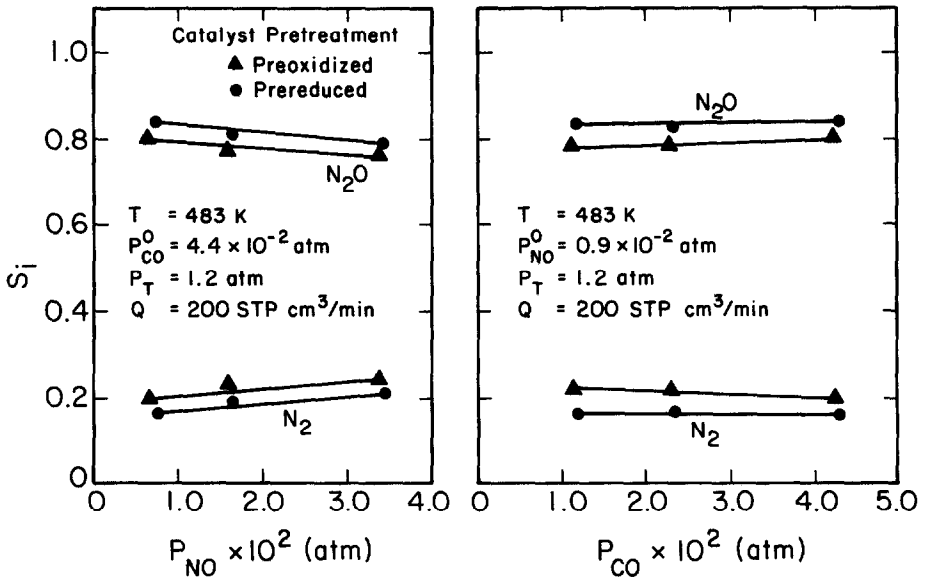

FIG. 2. Effect of pretreatment on the selectivities for N_2O and N_2.

treatment has only a small effect on product selectivity. Thus, N_2O selectivities are only 3 to 5% lower, and N_2 selectivities 3 to 5% higher, when the catalyst is preoxidized, rather than being prereduced. Reduction of a previously preoxidized catalyst resulted in a return to an activity and selectivity characteristic of a prereduced catalyst, indicating that the effects of pretreatment are reversible.

The dependence of the rate of NO reduction, and the rates of N_2O and N_2 formation, on the partial pressures of NO and CO were determined from runs 3, 4, and 5, listed in Table 1. The data from each of these runs were fit to power-law expressions of the form

$$N_i = k_i P_{CO}^{m_i} P_{NO}^{n_i}$$

where i = 1, 2, 3 correspond to NO, N_2O, and N_2, respectively; N_i is the turnover frequency for species i, k_i is the rate coefficient for species i; and m_i and n_i are the exponents on the partial pressures of CO and NO, respectively. A nonlinear regression technique was used to determine the parameter values which are listed in Table 2. Good fits between the power law model and the data were achieved in all cases, and the average deviation ranged between 1 and 2%.

Several observations can be made based on the information presented in Table 2. Variations in catalyst pretreatment and temperature influence the values of k_i but have little effect on the values of m_i and n_i. The values of m_i are all positive and lie in the range of 0.08 to 0.10. Thus, there is only a weak positive dependence on the partial

TABLE 1

Range of Operating Conditions for which Rate Data were Collected

Run	Pretreatment[a]	Temp (K)	Range of operating conditions		
			$P_{CO}^0 \times 10^2$ (atm)	$P_{NO}^0 \times 10^2$ (atm)	No. of data points
1	Red.	465–524	3.6	1.2	9
2	Oxid.	465–524	3.6	1.2	10
3	Red.	483	1.3–4.5	0.9–3.6	7
4	Red.	495	1.3–9.0	0.9–3.6	8
5	Oxid.	483	1.3–4.5	0.9–3.6	7
6	Red.	483	1.2–9.6	0.36–3.4	8
7	Red.	483	1.2–9.6	0.12–0.72	6

[a] Reduction was with 100% H_2 for 30–70 h at 553–573 K. Oxidation was with 1% NO for 1 h at 488 K.

TABLE 2

Power-Law Parameters for NO Reduction by CO

Run	Temp (K)	Pretreatment	$N_i = k_i P_{CO}^{m_i} P_{NO}^{n_i}$								
			N_2O			N_2			NO		
			$k_i \times 10^{3a}$	m_i	n_i	$k_i \times 10^{3a}$	m_i	n_i	$k_i \times 10^{3a}$	m_i	n_i
5	483	Oxid.	2.0	+0.08 ± 0.02	−0.23 ± 0.02	1.2	+0.08 ± 0.03	−0.06 ± 0.09	6.0	+0.08 ± 0.02	−0.20 ± 0.04
4	483	Red.	1.5	+0.08 ± 0.02	−0.21 ± 0.02	0.8	+0.07 ± 0.05	−0.05 ± 0.15	4.3	+0.08 ± 0.02	−0.17 ± 0.04
4A	495	Red.	3.4	+0.08 ± 0.02	−0.21 ± 0.02	1.6	+0.12 ± 0.03	−0.07 ± 0.08	9.8	+0.09 ± 0.02	−0.18 ± 0.04

[a] $[k_i] = \text{atm}^{-(m_i+n_i)}\ \text{s}^{-1}$.

pressure of CO, and it is virtually the same for NO reduction, N_2O formation, and N_2 formation. The values of n_i are negative in all cases. For NO reduction and N_2O formation, the values are approximately −0.20, but for N_2 formation the value is closer to −0.10.

Figure 3 illustrates the effects of temperature on the conversion of NO and the selectivities to N_2O and N_2 observed in Run 2. As the temperature is increased from 463 to 498 K, the NO conversion increases from 5 to 51%. At the same time, the selectivity to N_2O increases slightly from 0.76 to 0.81,

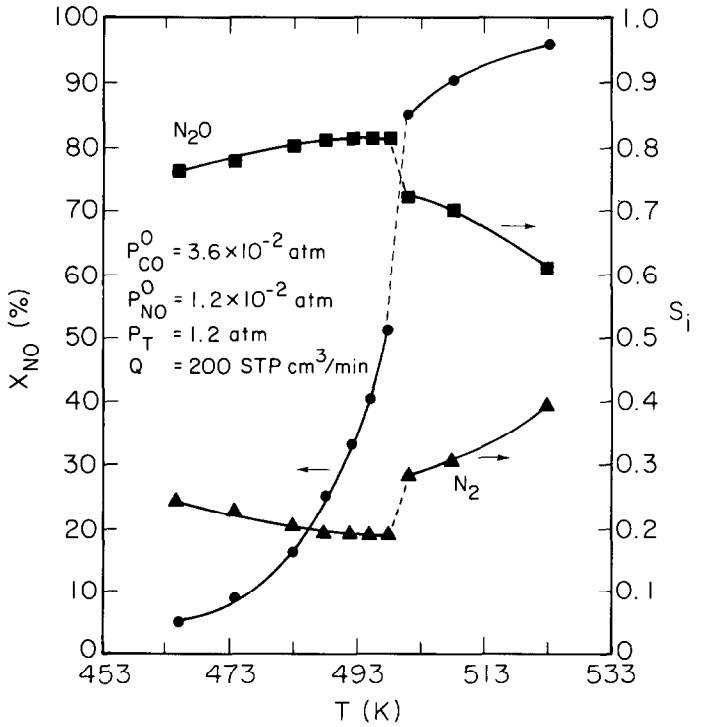

FIG. 3. Effect of temperature on NO conversion for a prereduced catalyst.

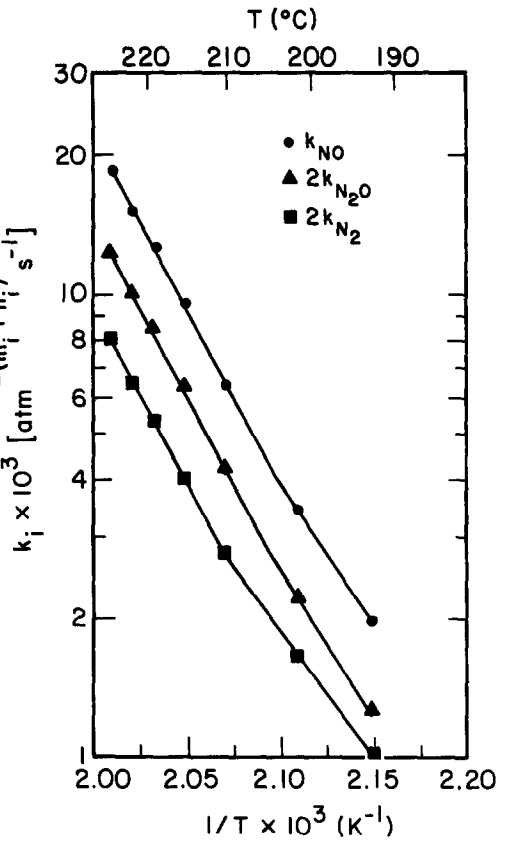

FIG. 4. Arrhenius plots for NO reduction and for N_2O and N_2 formation.

while the selectivity to N_2 decreases slightly from 0.24 to 0.19. When the temperature is increased from 498 to 501 K, the conversion increases from 51 to 85%. Concurrently, the selectivity to N_2O suddenly decreases, while the selectivity to N_2 suddenly increases. Increasing the temperature above 501 K causes the NO conversion to approach 100%. In this temperature range, the N_2O selectivity decreases and the N_2 selectivity increases with increasing temperature. Similar trends with temperature were observed in Run 1, with the exception that the conversion at a given temperature was lower. This pattern is consistent with the lower activity observed when the catalyst is prereduced, as opposed to being preoxidized.

The data from Run 2, for temperatures between 463 and 498 K, were used to determine the effects of temperature on the values of k_i appearing in Eq. (1). Figure 4 shows the dependence of k_i on temperature. At temperatures between 478 and 498 K, the data for NO reduction, N_2O formation, and N_2 formation fall along parallel straight lines characterized by an apparent activation energy of 33.5 kcal/mol. For temperatures below 478 K, the apparent activation energy for each species decreases. Based on the two data points for each species, in this temperature region, apparent activation energies of 27, 28, and 24 kcal/mol are calculated for NO, N_2O, and N_2, respectively.

An experiment was performed to assess the effect of space time, τ, on catalyst activity and selectivity. To avoid significant variations in reactant concentrations, the reaction conditions were chosen so that the NO conversion was always less than 10%. The results are shown in Fig. 5. As can be seen, variation of the space time over a sevenfold range had no effect on the distribution between N_2O and N_2 formation. This observation suggests that N_2O, once formed, does not undergo further reduction. Additional confirmation of this conclusion was obtained by studying the reaction between N_2O and CO. At a temperature of 499 K, a CO partial pressure of 3.6×10^{-2} atm, and an N_2O partial pressure of 6.0×10^{-3} atm, absolutely no reduction of N_2O could be detected.

Infrared Observations

A typical infrared spectrum obtained during the steady-state reduction of NO by CO is shown in Fig. 6. Similar spectra were observed for all of the reaction conditions used in this study. The primary differences between spectra were in the relative intensity of specific bands. For a few of the bands, a shift in frequency was also observed.

The bands observed at 2300 and 1465 cm^{-1} are associated with isocyanate species bound to the silica support. The positions

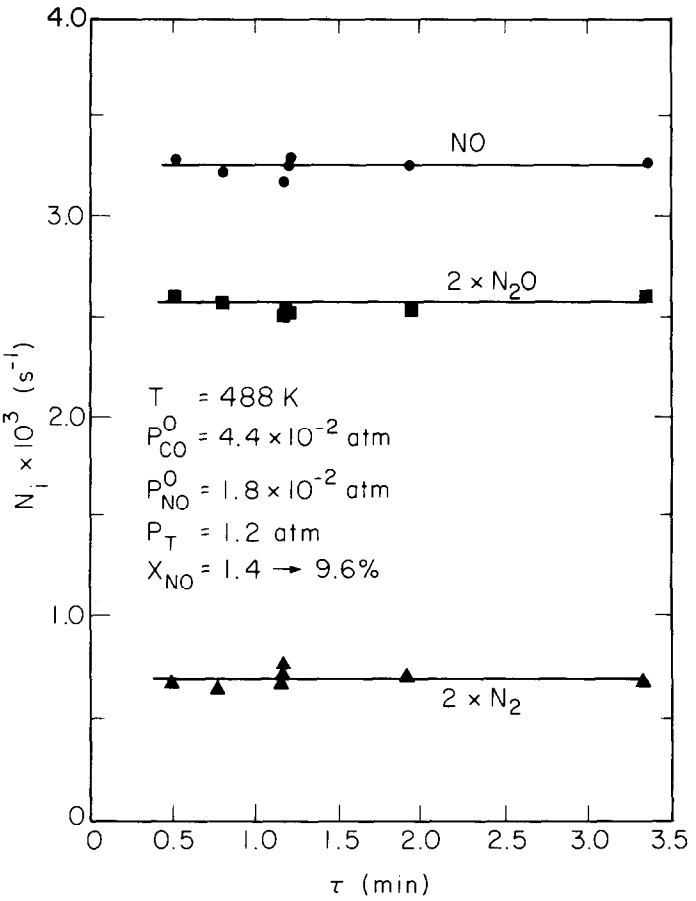

FIG. 5. Effect of space time on the turnover frequencies for NO reduction and for N_2O and N_2 formation.

of these bands correspond closely to the bands observed at 2284 and 1482 cm^{-1} for $Si(NCO)_4$ (*23*). The high frequency isocyanate band has also been observed in a number of earlier studies of NO reduction by CO over Rh and other Group VIII metals (*24–36*) and there is general agreement that the reported feature is ascribable to NCO species on the support. A more detailed presentation of the chemistry by which this species is formed and decomposed will be presented in a separate paper. Of primary significance for the present study is the observation that once formed the Si–NCO structure is extremely stable and appears not to participate in the NO reduction process.

The band at 2170 cm^{-1} can be assigned to a Rh–NCO species on the basis of the following factors. The first is that all transition metal isocyanate complexes exhibit bands between 2170 and 2230 cm^{-1} (*37–41*) due to asymmetric stretching of the NCO group. Similar bands have been observed when HNCO is decomposed on the surface of unsupported Pt (*42*). Evidence for M–NCO species has also been reported in studies of NO and CO coadsorption conducted with supported Ni (*30*), Ru (*29, 31*), and Rh (*35*) catalysts.

The bands at 2100 and 2040 cm^{-1}, seen in Fig. 6, are ascribed to the asymmetric and symmetric stretches of a rhodium dicarbonyl species. This assignment is based on

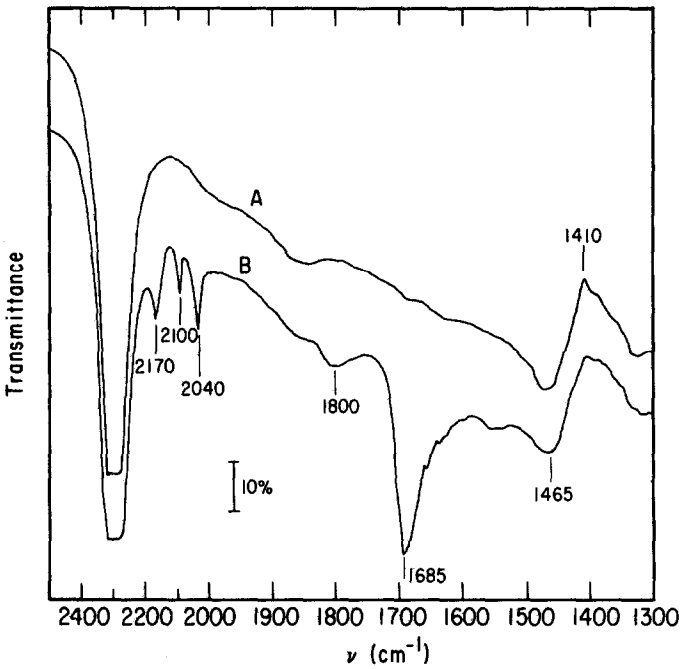

FIG. 6. Infrared spectra obtained during NO reduction by CO: (A) Baseline spectrum recorded at 493 K; (B) spectrum recorded under reaction conditions: $T = 488$ K, $P_{CO} = 3.4 \times 10^{-2}$ atm, $P_{NO} = 9.0 \times 10^{-3}$ atm, $x_{NO} = 25\%$.

infrared studies of CO adsorbed on silica- and alumina-supported Rh (*10–13*). At high NO conversions, and in the presence of excess CO, the band at 2040 cm^{-1} was observed to be significantly more intense than the band at 2100 cm^{-1}, and in several instances a new band could be observed at 2060 to 2070 cm^{-1}. This latter feature was also present when CO alone was contacted with the catalyst, and can be ascribed to a rhodium carbonyl structure of the form Rh–CO. Studies by Yates *et al.* (*11*) have shown that the band characteristic of Rh–CO shifts from 2070 cm^{-1} to lower frequencies as the CO coverage decreases from saturation. Thus, in instances where the band at 2040 cm^{-1} is more intense than that at 2100 cm^{-1}, it is quite possible that both the di- and monocarbonyl species are present on the surface together.

The intense band at 1685 cm^{-1} and the weak band at 1800 cm^{-1}, seen in Fig. 6, are both due to adsorbed NO. Similar bands were also observed when the catalyst was exposed to NO alone. The band at 1685 cm^{-1} is attributed to a negatively charged nitrosyl species, $Rh–NO^{\delta-}$, and the band at 1800 cm^{-1} to a neutral nitrosyl species, Rh–NO. These assignments are based on the similarity of the band positions to those observed in rhodium–nitrosyl complexes (*43–47*) and are consistent with those made in previous studies (*7, 8*) of the interaction of NO and CO on Rh.

The inverted band at 1410 cm^{-1} is an artifact resulting from an incomplete cancellation of the spectra for the catalyst and reference disks. The intensity of this feature was nearly constant and did not depend on the composition of the gas over the catalyst.

During Run 2, infrared spectra were obtained at eight different temperatures between 465 and 523 K. Four of these spectra are shown in Fig. 7. The spectra observed at 465 and 498 K are nearly identical, and

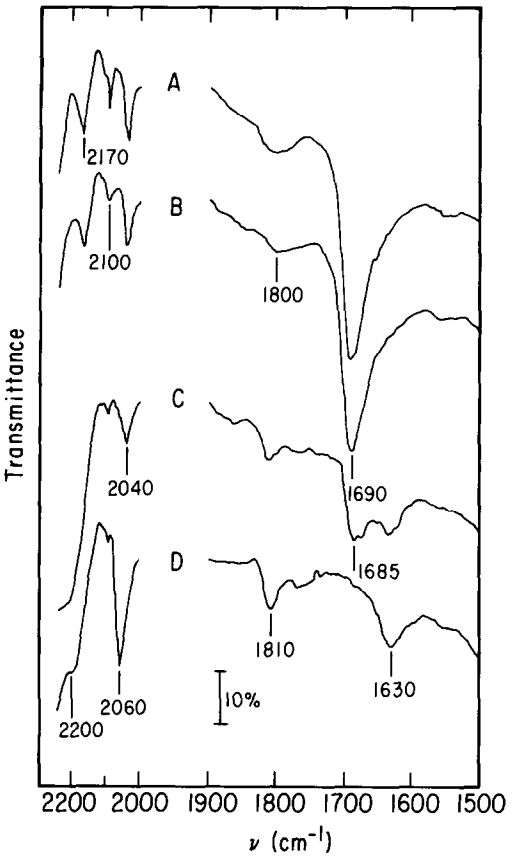

FIG. 7. Effect of temperature on the infrared spectra observed during NO reduction: $P_{CO}^0 = 3.6 \times 10^{-2}$ atm, $P_{NO}^0 = 1.2 \times 10^{-2}$ atm; (A) $T = 465$ K, $x_{NO} = 5\%$; (B) $T = 498$ K, $x_{NO} = 51\%$; (C) $T = 501$, $x_{NO} = 85\%$; (D) $T = 523$ K, $x_{NO} = 95\%$.

both are similar to the spectrum shown in Fig. 6. The NO conversion at 465 K is 5%, and is 51% at 498 K. When the temperature is raised to 501 K, the NO conversion increases to 85% and the spectrum of adsorbed species changes substantially relative to that seen at lower temperatures. The isocyanate band becomes much more intense and shifts upscale to 2200 cm^{-1}. The band at 1685 cm^{-1}, associated with Rh–$NO^{\delta-}$ becomes less intense, and a new feature appears at 1630 cm^{-1}. This latter band can also be assigned to a negatively charged nitrosyl. No significant changes are noted, though, in the intensities of the band at 1800 cm^{-1} for Rh–NO or the bands at 2100 and 2040 cm^{-1} for $Rh(CO)_2$. When the temperature is increased further to 523 K, the NO conversion increases to 96%. Figure 7 shows that at this temperature the bands at 1810–1800 and 1630 cm^{-1} become somewhat more intense, and the band at 1685 cm^{-1} disappears completely. These changes are indicative of the redistribution of NO species present on the Rh surface. The form of CO adsorption also changes, as is indicated by the appearance of an intense band at 2060 cm^{-1} characteristic of linearly adsorbed CO.

The effects of NO and CO partial pressure on the intensities of individual bands are illustrated in Figs. 8 and 9. Figure 8 shows that as the partial pressure of NO is decreased, the Rh–NO band at 1800 cm^{-1} decreases in intensity monotonically. The Rh–$NO^{\delta-}$ band at 1685 cm^{-1} remains constant for NO partial pressures down to 4×10^{-3} atm, but decreases slightly thereafter. The band at 2040 cm^{-1} is unaffected by the NO partial pressure for partial pressures above about 10^{-2} atm. Below this value, the band intensity begins to increase. While not shown, the intensity of the band at 2100 cm^{-1} remains constant throughout the range of NO partial pressures considered. This suggests that the increase in the intensity of the band at 2040 cm^{-1} for NO partial pressures below 10^{-2} atm is due to an increasing coverage by Rh–CO species, rather than to an increase in the coverage by $Rh(CO)_2$ species. Finally, the Rh–NCO band at 2170 cm^{-1} is seen to be relatively insensitive to the NO partial pressure.

Figure 9 illustrates the influence of CO partial pressure on the Rh–$NO^{\delta-}$ and Rh–NCO bands, at 1685 and 2170 cm^{-1}, respectively. The intensity of the band at 2170 cm^{-1} is relatively insensitive to the CO partial pressure, whereas the band at 1685 cm^{-1} decreases slowly with increasing CO partial pressure. The bands appearing at 2100, 2040, and 1800 cm^{-1} were all unaffected by the variations in the CO partial pressure over the range indicated in Fig. 9.

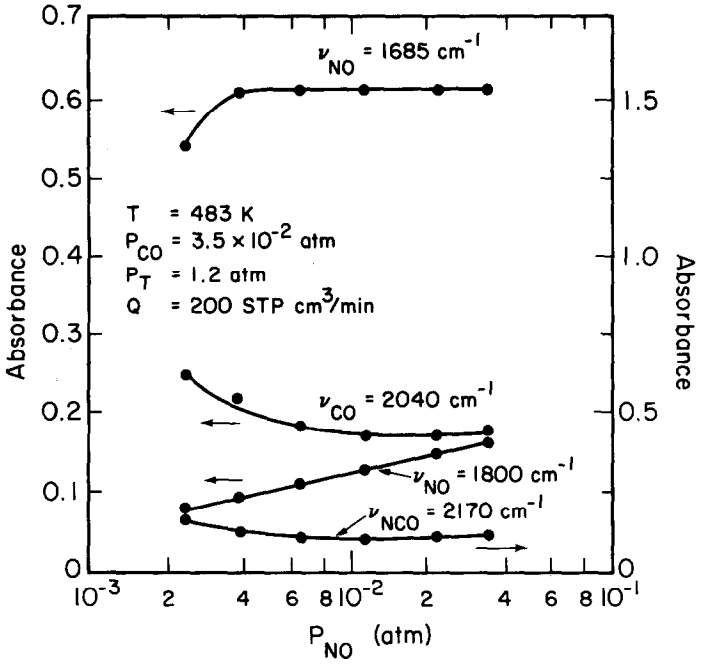

FIG. 8. Effect of NO partial pressure on the absorbances of the infrared bands for NO, CO, and NCO.

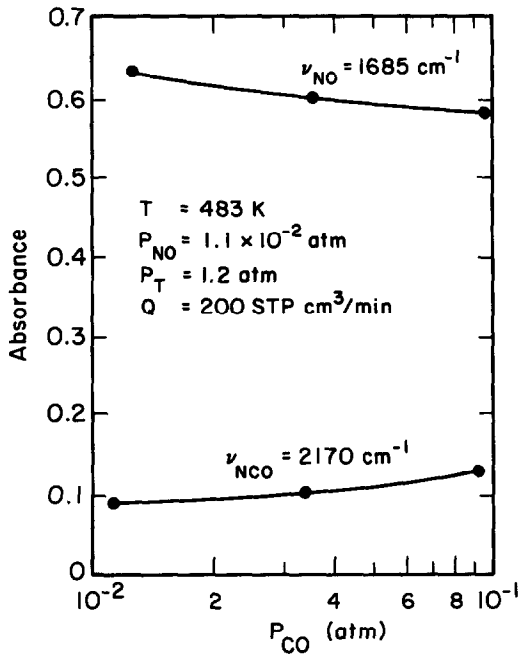

FIG. 9. Effects of CO partial pressure on the absorbances of the infrared bands for NO and NCO.

DISCUSSION

For NO conversions of less than 50%, the results of the present experiments indicate that the kinetics of NO reduction and the kinetics of N_2O and N_2 formation are very similar, both in regard to the power law dependencies on the partial pressures of NO and CO, and the global activation energies. These features can be rationalized in terms of the reaction sequence shown below, which is based on published information concerning the interactions of NO and CO with Rh surfaces.

1. $NO + S \rightleftarrows NO_a$
2. $CO + S \rightleftarrows CO_a$
3. $NO_a + S \rightarrow N_a + O_a$
4. $NO_a + N_a \rightarrow N_2O + 2S$
5. $NO_a + N_a \rightarrow N_2 + O_a + S$
6. $CO_a + O_a \rightarrow CO_2 + 2S$

Reaction 1 represents the reversible, associative adsorption of NO. As indicated by the infrared spectra obtained here and in

previous studies (*7, 8*), molecularly adsorbed NO is the dominant species present on the surface during the reduction of NO by CO. The reversibility of NO adsorption on Rh has recently been examined by Savatsky and Bell (*9*). Their work shows that the exchange of gas-phase and adsorbed NO is very rapid and proceeds at a much faster rate than that for NO reduction.

The adsorption of molecular CO, reaction 2, is evidenced by the presence of the infrared band at 2040 cm^{-1}, seen in Figs. 7 and 8. Studies reported by Yates *et al.* (*11*) indicate that the exchange of gas-phase and adsorbed CO is very rapid, and, hence, that the adsorption of CO can be viewed as being reversible.

Temperature-programmed desorption studies carried out with both supported and unsupported Rh have shown that at elevated temperatures adsorbed NO readily undergoes dissociation to form N and O atoms, reaction 3 (*14–17*). Chin and Bell (*14*) have recently estimated the activation energy for this process to be about 8 kcal/mol. The form of adsorbed NO (viz., $Rh–NO^{\delta-}$, Rh–NO, $Rh–NO^{\delta+}$) which undergoes dissociation most readily has not been established, but it is likely to be $Rh–NO^{\delta-}$ since this species has the weakest N–O bond. For the purpose of the present discussion, though, no distinctions are made between the different forms of adsorbed NO.

The formation of N_2O is assumed to occur via a Langmuir–Hinshelwood process, as illustrated by reaction 4. Evidence for the occurrence of this reaction comes primarily from recent investigations of the temperature-programmed decomposition of adsorbed NO (*14*). These studies also suggest that N_2 is formed via reaction 5. While N_2 can also be formed by the recombination of two N atoms, this process is characterized by a higher activation energy than that for reaction 5 (*14, 15*).

Reaction 6 describes the removal of adsorbed O atoms from the catalyst surface by reaction with adsorbed CO. Campbell and White (*16*) have shown that this process occurs much more rapidly than the reaction of gas-phase CO with adsorbed O atoms.

Studies of the formation and decomposition of Rh–NCO, which are to be reported separately, suggest that this species is not directly involved in the formation of the reaction products. As a consequence, steps involving Rh–NCO have not been incorporated into the reduction mechanism proposed above. It is also noted that for NO conversions below 50%, the infrared spectra shown in Figs. 7 and 8, indicate that the surface coverage by Rh–NCO is small compared to the coverages by adsorbed NO.

Based on the mechanism represented by reactions 1 through 6, rate expressions can be derived for the kinetics of NO reduction and the kinetics of N_2O and N_2 formation. Before proceeding, it is desirable to introduce several assumptions. The first is that the rates of NO and CO adsorption and desorption are much more rapid than the rate of NO reduction, and, hence, that the surface coverage by both reactants can be represented by equilibrium expressions. This assumption is supported by estimates of the rates of NO and CO desorption from Rh, using experimentally determined rate parameters (*9*). In the temperature range of 473 to 508 K, it is determined that the rates of NO and CO desorption are 10^4 to 10^5 times faster than the rate of NO reduction. The second assumption is that reaction 3 is the rate-limiting step in the mechanism. This assumption is supported by the temperature-programmed desorption studies of Campbell and White (*16*), and Chin and Bell (*14*), and the theoretical calculations of Miyazaki and Yasumori (*48*).

The turnover frequency for NO reduction, N_{NO}, can be expressed as

$$N_{NO} = k_3\theta_{NO}\theta_v \qquad (1)$$

where k_3 is the rate coefficient for reaction 3, and θ_{NO} and θ_v are the fractional surface coverages for adsorbed NO and vacancies, respectively. If it is assumed that the sur-

face coverage by adsorbed NO and CO are described by Langmuir isotherms, then it follows that

$$\theta_{NO} = K_1 P_{NO} \theta_v \quad (2)$$

and

$$\theta_{CO} = K_2 P_{CO} \theta_v \quad (3)$$

where P_{NO} and P_{CO} are the partial pressures of NO and CO, and K_1 and K_2 are the equilibrium constants associated with reactions 1 and 2. Substitution of Eq. (2) into Eq. (1) and imposition of a steady-state balance on Rh surface sites, leads to the following expression for N_{NO}:

$$N_{NO} = \frac{k_3 K_1 P_{NO}}{[1 + K_1 P_{NO} + K_2 P_{CO} + k' P_{NO}/P_{CO} + k'']^2} \quad (4)$$

where

$$k' = \frac{k_3 K_1}{k_6 K_2} \frac{k_4 + 2k_5}{k_4 + k_5} \quad (5)$$

and

$$k'' = k_3/(k_4 + k_5) \quad (6)$$

In Eqs. (4) through (6), k_i represents the rate coefficient for reaction i. The second and third terms in the denominator of Eq. (4) arise from the coverage of the Rh surface by NO and CO, respectively, whereas the fourth and fifth terms in the denominator of Eq. (4) are due to the coverages by N and O atoms.

Under steady-state reaction conditions, the infrared spectra presented in Figs. 6 and 7 suggest that the surface is dominated by adsorbed NO and that the coverage by adsorbed CO is significantly less than that of NO. Nothing can be said about the coverages by N and O atoms, but these are not expected to be large since the atomic species are highly reactive. Based on these considerations, it is reasonable to conclude that the second term in the denominator of Eq. (4) dominates over the rest. Under such circumstances, Eq. (4) can be approximated by Eq. (7)

$$N_{NO} = \frac{k_3}{K_1 P_{NO}} \quad (7)$$

Equation (7) is of the form of a power-law rate expression and can be compared directly with the power-law rate expression deduced from experimental results (see Table 2). The empirical dependence on CO partial pressure is +0.08 order, whereas Eq. (7) indicates a zero-order dependence. The complete absence of any dependence on CO partial pressure in Eq. (7) is due to the assumption that the surface coverages by CO and O are negligible. If the latter assumption is relaxed somewhat, then it is apparent from the form of Eq. (4) that a positive order dependence on CO will appear in the rate expression for the NO reduction.

It is also noted that while Eq. (7) predicts an inverse first-order dependence on NO, the observed dependence is −0.20. A possible reason for this discrepancy might be the assumption that θ_{NO} is described by a Langmuir isotherm. As an alternative, it is useful to consider describing θ_{NO} as function of P_{NO} using the infrared data presented in Fig. 8. For this purpose, no distinction is made between the species absorbing at 1680 and 1800 cm^{-1}, and it is assumed that the extinction coefficients for both species are identical and neither coefficient is dependent on NO coverage. If it is further assumed that $\theta_{NO} = 0.90$ at $P_{NO} = 3.5 \times 10^{-2}$ atm, then the dependence of θ_{NO} on P_{NO} can be described by

$$\theta_{NO} = 0.70 + 0.50 P_{NO}^{0.27} \quad (8)$$

The first term on the right-hand side of Eq. (8) represents the coverage by $NO_a^{\delta-}$ and the second the coverage by NO_a. It should be noted that in the formulation of Eq. (8), no provision was made for the dependence of θ_{NO} on P_{CO}. This decision is justified by the fact that the data in Fig. 9 show only a weak inverse dependence of θ_{NO} on P_{CO}.

Since the rate of NO dissociation controls the rate of NO reduction, N_{NO} can be written as

$$N_{NO} = k_3\theta_{NO}\theta_v \simeq k_3\theta_{NO}(1 - \theta_{NO}) \quad (9)$$

Substitution of Eq. (8) into Eq. (9) gives

$$N_{NO} = k_3(0.70 + 0.50P_{NO}^{0.27})(0.30 - 0.50P_{NO}^{0.27}) \quad (10)$$

Equation (10) can now be represented as a power-law expression, over a narrow range of NO partial pressures. When this is done for values of P_{NO} between 5.0×10^{-3} and 3.0×10^{-2} atm, the following expression results

$$N_{NO} = kP_{NO}^{-0.24} \quad (11)$$

Here, k is the apparent rate coefficient for NO reduction. Equation (11) is in excellent agreement with the rate expression determined from measured rate data. This suggests that the infrared data provide a more accurate representation of NO coverage than that given by a Langmuir isotherm. It is noted, though, that this conclusion depends on the validity of the assumptions made in deriving Eq. (8), none of which have been confirmed.

Based on the proposed mechanism, the rates of N_2O and N_2 formation are given by

$$N_{N_2O} = \frac{0.5k_4}{(k_4 + k_5)} N_{NO} \quad (12)$$

$$N_{N_2} = \frac{0.5k_5}{(k_4 + k_5)} N_{NO} \quad (13)$$

Equations (12) and (13) indicate that the dependencies of N_2O and N_2 formation on the partial pressures of NO and CO are identical to those for the overall consumption of NO. Inspection of Table 2 shows that this is consistent with observed experimental observation.

The data presented in Fig. 4 demonstrate that the activation energies for N_2O and N_2 formation are equivalent and identical to the activation energy for NO consumption. To be consistent with observation, the forms of Eqs. (12) and (13) require that $E_4 = E_5$. In a recent study of the decomposition of NO adsorbed on silica-supported Rh, Chin and Bell (*14*) determined that the activation energies for reactions 4 and 5 are indeed equivalent. The consistency of those results with the data presented here lends further support to the proposition that the selectivity of Rh for N_2O and N_2 formation is properly described by reactions 4 and 5.

Preoxidation of the catalyst with NO was observed to give steady-state NO reduction rates which were approximately 50% higher than those obtained following prereduction with H_2 (see Fig. 1). However, the nature of the pretreatment was seen to have little effect on either product selectivity or the concentrations of species observable by infrared spectroscopy. Effects of pretreatment have been seen previously on Rh and other noble metals. Amariglio *et al.* (*49*) have reported that preoxidation of a Rh ribbon increased its activity for ethylene hydrogenation. Taylor *et al.* (*50*) have found that preoxidation enhanced the NO reduction activity of both Pt/Al_2O_3 and Pd/Al_2O_3, but not Ru/Al_2O_3. They noted, however, that on Ru/Al_2O_3 preoxidation enhanced the N_2 selectivity. They also concluded that the effects of pretreatment were not a simple function of catalyst dispersion.

It is interesting to speculate on why the catalyst used in this study is more active following preoxidation than prereduction. Since the activity is enhanced without affecting selectivity, it is reasonable to suggest that the primary influence of pretreatment is on reaction 3, the rate-limiting step, rather than on reactions 4 or 5. Reaction 3 involves the cleavage of the N–O bond in adsorbed NO, to form Rh–N and Rh–O. The progress of this reaction is very likely to be influenced by the degree of charge transfer from the Rh to the antibonding π^* orbital of the adsorbed NO and by Lewis-acid/base type interactions occurring between the oxygen end of the adsorbate and

the catalyst surface. The infrared spectra obtained in this study indicate that, independent of catalyst pretreatment, the dominant adsorbed species is Rh–$NO^{\delta-}$. The low N–O stretching frequency for this structure relative to gas-phase NO indicates that the N–O bond is weakened and suggests that NO adsorbed as Rh–$NO^{\delta-}$ is predisposed to dissociation. Further facilitation of NO dissociation might be envisioned to occur through the interaction of the negatively charged oxygen end of the nitrosyl group with a Lewis-acid site on the metal surface. Such sites might occur as positively charged Rh atoms produced during preoxidation of the catalyst. This idea is supported by recent studies (*51–54*) of the interactions of oxygen with Rh, which show that oxygen atoms can penetrate below the metal surface and become strongly bound. Such subsurface oxygen is resistant to reduction at temperatures below 600 K. The presence of subsurface oxygen would certainly modify the electronic properties of Rh atoms in the surface layer and might, by the means described above, account for the more facile dissociation of NO over the preoxidized catalyst. While the proposed interpretation is admittedly speculative, it does explain why the higher activity of the preoxidized catalyst is stable and does not revert to that characteristic of the prereduced catalyst, even after extended use for NO reduction under conditions where the reacting gas has a stoichiometric excess of CO over NO.

An alternative, and of course simpler explanation for the higher activity of the preoxidized catalyst, is that the Rh surface area for such a catalyst is higher than that for a prereduced catalyst. While no attempt was made to measure the dispersion of the preoxidized catalyst, an investigation of the effects of oxidation and reduction on the dispersion of silica-supported Rh conducted by Wang and Schmidt (*55*) suggests that this explanation is probably not correct. In that study, the authors reported that oxidation in air at temperatures in excess of 773 K was required to achieve significant redispersion of Rh on SiO_2. In the present study, oxidation was carried out at 423 K. At such a low temperature, it is unlikely that the supported Rh microcrystallites would have been converted extensively to Rh_2O_3, one of the requirements for Rh redispersion (*55*).

CONCLUSIONS

The activity of silica-supported Rh for NO reduction by CO has been found to be sensitive to the nature of the catalyst pretreatment. Preoxidation in NO increases the specific activity for NO reduction by 50% over that observed when the catalyst is prereduced. Pretreatment conditions have little effect, though, on the selectivity for forming N_2 versus N_2O. Likewise, pretreatment conditions do not influence the dependence of the reaction kinetics on the partial pressures of NO and CO, nor on temperature.

The kinetics for NO reduction, and for N_2 and N_2O formation, were determined for conditions where the NO conversion is less than 50%. In all cases, the reaction rates exhibit a weak, positive order dependence on CO partial pressure and a moderate, inverse order dependence on NO partial pressure. The activation energies for all three reactions are equivalent. Of further significance is the observation that the selectivity for N_2O formation is independent of gas space velocity, and only weakly dependent on reactant concentrations and catalyst temperature. This strongly suggests that N_2 and N_2O are formed via common pathways.

Infrared observations indicate that for NO conversions below 50%, the catalyst surface is dominated by adsorbed NO. Two structures are identified. The major one is Rh–$NO^{\delta-}$ and the minor one is Rh–NO. Small concentrations of adsorbed CO, as Rh–CO, and isocyanate groups, Rh–NCO, are also observed. At NO conversions in excess of 50%, and in the presence of stoichiometric excess of CO, the intensities of the CO and NCO bands become much more

pronounced than those observed at lower NO conversions. Variation of the NO and CO partial pressures under conditions of low NO conversion (<50%) indicate that NO coverage increases with increasing P_{NO} and decreases somewhat with increasing P_{CO}, suggesting competitive adsorption of the two reactants.

The kinetics and infrared spectra observed in this study can be interpreted on the basis of a relatively simple reaction mechanism. Both NO and CO are assumed to adsorb reversibly. The dissociation of molecularly adsorbed NO is taken to be the rate-limiting step. N_2O formation is assumed to occur via the process $N_a + NO_a \rightarrow N_2O + 2S$ and N_2 formation by the related process $N_a + NO_a \rightarrow N_2 + O_a + S$. Atomically adsorbed oxygen is removed from the surface by reaction with adsorbed CO. Rate expressions derived on the basis of this mechanism are qualitatively consistent with those obtained from experimental data. The agreement between the observed and predicted dependence on NO partial pressure can be improved by using the infrared data to describe the coverage of the catalyst surface by NO, rather than assuming a Langmuir isotherm. Finally, it is suggested that the increase in the rate of NO reduction caused by preoxidation of the catalyst might be ascribed to the presence of cationic rhodium sites. Such sites would be capable of participating in Lewis acid–base interactions with the oxygen end of adsorbed NO, thereby facilitating dissociation of the N–O bond.

ACKNOWLEDGMENT

This work was supported by the NSF under Grant CPE-7826352.

REFERENCES

1. Hegedus, L. L., and Gumbleton, J. J., *Chemtech* **10,** 630 (1980).
2. Kobylinski, T. P., and Taylor, B. W., *J. Catal.* **33,** 376 (1974).
3. Schlatter, J. C., and Taylor, K. C., *J. Catal.* **49,** 42 (1977).
4. Shelef, M., and Kummer, J. T., *Chem. Eng. Prog. Symp. Ser.* **67,** 74 (1971).
5. Shelef, M., *Cat. Rev. Sci. Eng.* **11,** 1 (1975).
6. Wei, J., "Advances in Catalysis," Vol. 27, p. 57. Academic Press, New York, 1975.
7. Arai, H., and Tominaga, H., *J. Catal.* **43,** 131 (1976).
8. Solymosi, F., and Sarkany, J., *Appl. Surf. Sci.* **3,** 68 (1979).
9. Savatsky, B. J., and Bell, A. T., *ACS Symp. Ser.* **178,** 105 (1982).
10. Yang, A. C., and Garland, C. W., *J. Phys. Chem.* **61,** 1504 (1957).
11. Yates, J. T., Duncan, T. M., Worley, S. D., and Vaughn, R. W., *J. Chem. Phys.* **70**(03), 1219 (1979).
12. Cavanagh, R. R., and Yates, J. T., *J. Chem. Phys.* **74**(7), 4150 (1981).
13. Rice, C. A., Worley, S. D., Curtis, C. W., Guin, J. A., and Tarrer, A. R., *J. Chem. Phys.* **74,** 6487 (1981).
14. Chin, A. A., and Bell, A. T., *J. Phys. Chem.*, in press.
15. Castner, D. G., Sexton, B. A., and Somorjai, G. A., *Surf. Sci.* **71,** 519 (1978).
16. Campbell, C. T., and White, J. M., *Appl. Surf. Sci.* **1,** 347 (1978).
17. Baird, R. J., Ku, R. C., and Wynblatt, P., *Surf. Sci.* **97,** 346 (1980).
18. London, J., and Bell, A. T., *J. Catal.* **31,** 32 (1973).
19. Lorimer, D., and Bell, A. T., *J. Catal.* **59,** 223 (1979).
20. Hicks, R. F., Kellner, C. S., Savatsky, B. J., Hecker, W. C., and Bell, A. T., *J. Catal.* **71,** 216 (1981).
21. Hecker, W. C., Ph.D. thesis, University of California, Berkeley, 1982.
22. Hecker, W. C., and Bell, A. T., *Anal. Chem.* **53,** 817 (1981).
23. Miller, F. A., and Carlson, G. A., *Spectrachim. Acta.* **17,** 977 (1961).
24. London, J., and Bell, A. T., *J. Catal.* **31,** 96 (1973).
25. Unland, M. L., *Science* **179,** 567 (1973).
26. Unland, M. L., *J. Phys. Chem.* **77,** 1952 (1973).
27. Unland, M. L., *J. Catal.* **31,** 459 (1973).
28. Dalla Betta, R. A., and Shelef, M., *J. Mol. Catal.* **1,** 431 (1976).
29. Brown, M. F., and González, R. D., *J. Catal.* **44,** 477 (1976).
30. Morrow, B. A., and Moran, L. E., *J. Phys. Chem.* **81,** 2667 (1977).
31. Davydov, A. A., and Bell, A. T., *J. Catal.* **49,** 345 (1977).
32. Voorhoeve, R. J. H., Trimble, L. E., and Freed, D. J., *Science* **200,** 759 (1978).

33. Voorhoeve, R. J. H., Trimble, L. E., *J. Catal.* **54,** 269 (1978).
34. Solymosi, F., and Bansagi, T., *J. Phys. Chem.* **83,** 552 (1979).
35. Solymosi, F., and Sarkany, J., *Appl. Surf. Sci.* **3,** 68 (1979).
36. Rasko, J., and Solymosi, F., *J. Catal.* **71,** 219 (1981).
37. Forster, D., and Goodgame, D. M. L., *J. Chem. Soc.* 262 (1965).
38. Chugtai, A. R., and Keller, R. N., *J. Inorg. Nucl. Chem.* **31,** 633 (1969).
39. Forster, D., and Goodgame, D. M. L., *J. Chem. Soc.* 1286 (1965).
40. Norbury, A. H., and Sinha, A. I. P., *J. Chem. Soc. A* 1598 (1968).
41. Anderson, S. J., and Norbury, A. H., *Chem. Commun.* 37 (1974).
42. Gorte, R. J., Schmidt, L. D., and Sexton, B. A., *J. Catal.* **67,** 387 (1981).
43. Feltham, R. D., and Enemark, H. J., *in* "Topics in Stereochemistry" (G. L. Geoffrey, Ed.), Vol. 12. Wiley, New York, 1978.
44. Dubois, L. H., Hansma, P. K., and Somorjai, G. A., *J. Catal.* **65,** 318 (1980).
45. Cotton, F. A., and Wilkinson, G., "Advanced Inorganic Chemistry." 4th ed. Wiley, New York, 1980.
46. Nakamoto, K., "Infrared and Raman Spectra of Inorganic and Coordination Compounds." 3rd ed. Wiley, New York, 1978.
47. Pierpont, C. G., VanDerveer, D. G., Durland, W., and Eisenberg, R., *J. Amer. Chem. Soc.* **92,** 4760 (1970).
48. Miyazaki, E., and Yasumori, I., *Surf. Sci.* **57,** 755 (1976).
49. Amariglio, A., Lakhdar, M., and Amariglio, H., *in* "Proceedings, 7th International Congress on Catalysis, Tokyo," p. 669. Elsevier, New York, 1981.
50. Taylor, K. C., Sinkevitch, R. M., and Klimisch, R. L., *J. Catal.* **35,** 34 (1974).
51. Campbell, C. T., and White, J. M., *Appl. Surf. Sci.* **1,** 347 (1978).
52. Thiel, P. A., Yates, Jr., Y. T., and Weinberg, W. H., *Surf. Sci.* **90,** 121 (1979).
53. Castner, D. G., Ph.D. thesis, Department of Chemistry, University of California, Berkeley, 1979.
54. Gorodetskii, V. D., Nieuwenhuys, B. E., Sachtler, W. M. H., and Boreskov, G. K., *Appl. Surf. Sci.* **7,** 355 (1981).
55. Wang, T., and Schmidt, L. D., *J. Catal.* **70,** 187 (1981).